resembles very much that of *E. coli* (Ueki, Tanaka, Nakae & Nikaido, 1979), the agreement of the results from X-ray and electron microscopy indicates that the interpretation of $A_0(u)$ is correct. The model construction of the protein assembly from $A_0(u)$ with threefold rotational symmetry was carried out and we have obtained a reasonable model structure of the assembly (Ueki, Tanaka & Nakae, 1979).

For the equatorial diffraction from chromatophore of *Rhodospirillum rubrum*, the method using the radial autocorrelation function was applied. Although we have reported that equatorial reflections could be indexed as a two-dimensional hexagonal lattice with $a = 42{\cdot}6$ Å (Ueki, Kataoka & Mitsui, 1976), the radial autocorrelation function suggests that the protein assembly is not crystalline but has rotational symmetry. Details will be published elsewhere (Kataoka & Ueki, 1979).

### References


BLAUROCK, A. E. (1975). *J. Mol. Biol.* **93**, 139–158.

BLAUROCK, A. E. & STOECKENIUS, W. (1971). *Nature (London) New Biol.* **233**, 152–155.

BUERGER, M. J. (1959). *Vector Space and its Application in Crystal-Structure Investigation.* New York: John Wiley.

EARNSHAW, W., CASJENS, S. & HARRISON, S. C. (1976). *J. Mol. Biol.* **104**, 387–410.

FRANKLIN, R. E. & KLUG, A. (1955). *Acta Cryst.* **8**, 777–780.

HENDERSON, R. (1975). *J. Mol. Biol.* **93**, 123–138.

KATAOKA, M. & UEKI, T. (1979). In preparation.

MACGILLAVRY, C. H. & BRUINS, E. M. (1948). *Acta Cryst.* **1**, 156–158.

OSTER, G. & RILEY, D. P. (1952). *Acta Cryst.* **5**, 272–276.

POROD, G. (1951). *Kolloid Z.* **124**, 83–114.

SMIT, J., KAMIO, Y. & NIKAIDO, H. (1976). *J. Bacteriol.* **124**, 942–958.

STEVEN, A. C., HEGGELER, B., MILLER, R., KISTLER, J. & ROSENBUSCH, J. P. (1977). *J. Cell Biol.* **72**, 292–301.

UEKI, T., KATAOKA, M. & MITSUI, T. (1976). *Nature (London)*, **262**, 809–810.

UEKI, T., MITSUI, T. & NIKAIDO, H. (1979). *J. Biochem. (Tokyo)*, **85**, 173–182.

UEKI, T., TANAKA, M. & NAKAE, T. (1979). In preparation.

UEKI, T., TANAKA, M., NAKAE, T. & NIKAIDO, H. (1979). In preparation.

UNWIN, P. N. T. & HENDERSON, R. (1975). *J. Mol. Biol.* **94**, 425–440.

VAINSHTEIN, B. K. (1966). *Diffraction of X-rays by Chain Molecules.* Amsterdam: Elsevier.

WASER, J. (1955). *Acta Cryst.* **8**, 142–150.


*Acta Cryst.* (1980). A**36**, 287–295

# The Physical Foundations of the Computer Simulation of X-ray Traverse Topographs


BY P. V. PETRASHEN'*

*Physical-Technical Institute, Academy of Sciences of the USSR, Leningrad, USSR*

F. N. CHUKHOVSKII

*Institute of Crystallography, Academy of Sciences of the USSR, Moscow, USSR*

AND I. L. SHULPINA

*Physical-Technical Institute, Academy of Sciences of the USSR, Leningrad, USSR*


(*Received* 1 *December* 1978; *accepted* 18 *October* 1979)


## Abstract

A general problem of the computer simulation of X-ray traverse topographs is treated on the basis of the Green-function method. Special attention is paid to the role of partial coherence of the incident radiation and to the problem of accounting for it in the practical calculations. The reciprocity theorem for the Green functions is proved rigorously in the X-ray diffraction optics and is applied to solve the problem in question. Different approaches based on the solution of the boundary problem of the Cauchy type and on the Green-function method are analysed and are compared from the view point of the computation time needed and of their adaptation capability to real experimental conditions. It is shown that, in the present case of a small correlation length in the primary beam, the Green function method has very significant advantages, which make it the only one acceptable for practical computer


* Present address: VNII Nauch Pribor, Stakhanovtsev Street 1, 195112, Leningrad, USSR.

0567-7394/80/020287-09$01.00

simulations. As examples, the diffracted intensity profiles of some dislocation images are computed with this method. These profiles demonstrate good correspondence with the experimental ones as well as the possibility of the determination of the Burgers vector sign from the pairs of profiles measured with opposite directions of the diffraction vector.

## 1. Introduction

Amongst the methods of the X-ray topography of single crystals, X-ray traverse topography (XTT) is the most widespread so far, since information about the defect distribution in a large volume of a crystal may be obtained in a relatively short time (Lang, 1959). From the type of diffraction image, it is also possible to determine what kind of defect is visible – dislocation, dislocation loop, stacking fault, *etc.* Furthermore, the shape and location of the direct (projection) image yields some geometrical information about a defect. In particular, the geometrical parameters of the straight-line dislocation cutting both the crystal faces may be easily reconstructed (Authier, 1967). In the case when a defect lies in the bulk of a crystal its depth beneath the surface is estimated approximately from the image width and some features of the contrast details. More particular information (the Burgers vector direction, for example) is available from a number of the topographs, taken for different reflections at the same time, although the sign of the Burgers vector remains uncertain.

Thus, up to now XTT is still not capable of yielding the total information about single defects. A decisive improvement, in principle, in this field could be achieved by the use of quantitative methods of image study. As regards X-ray section topography (XST; Kato & Lang, 1959), such an approach has been known for more than ten years (Balibar & Authier, 1967; Epelboin, 1974). The XST image of any chosen defect is numerically simulated rather easily, so that a quantitative comparison of the experimental image with the computed one is available in order to check the defect model and to determine all the parameters of the defect involved. For this reason, XST is often used when complete defect data are needed. However, it should be kept in mind that because of a small illuminated volume and very long exposure time XST is as yet no good in practice for the investigation of single crystals with large volume.

It is obvious that computer-technique development for XTT image simulation would lead to a better understanding of the formation of the diffracted images themselves and to a significant increase in the amount of information received from XTT. However, such a problem is much more complicated in comparison with the simulation of XST or double-crystal topographs. The main difficulty is the space and time incoherence of the incident radiation as well as the large dimensions of the illuminated crystal area. The computer simulation of defect images in the approximation of an X-ray monochromatic plane wave falling on a crystal surface does not explain the XTT experiments (Chukhovskii & Shtolberg, 1970, 1973). A true picture could be obtained by averaging the diffracted image over the set of plane waves or representing the incident X-ray bundle by a number of mutually independent point sources on the entrance surface of a crystal (it will be shown below that these two methods are the particular cases of a more general approach). These approaches are not efficient for practical purposes because of the long computer time needed and the low accuracy of calculations, as was shown by Epelboin (1977).

Up to now, the only computer simulations of XTT images have been carried out for the case of a stacking fault in a crystal when the greater part of the calculation is feasible in an analytical form (Wonciewicz & Patel, 1975, 1976). Wonciewicz & Patel obtained an interesting result, namely that the behaviour of the interference fringes on the XTT fault image differs from that on the XST image; in particular, the sign of the first fringe from the exit surface may be either the same as on the XST pattern or reversed depending on the diffraction conditions and the defect geometry. This example shows that the contrast formation, in general, is different for these two topographic methods and the XTT images should be studied separately. Such studies are clearly impossible without appropriate methods and systematic computer simulations.

The computer simulation problem of XTT consists of two major points: the first is a general physical treatment of the problem and the choice of a rational scheme of calculation; the second is the development of a suitable numerical method. The present paper deals mainly with the first point. An effective numerical method for the problem has been proposed by one of the authors (Petrashen', 1976). A new approach to the problem is based on the Green-function formulation of the X-ray diffraction theory (§§ 2, 3) and the reciprocity theorem which is proved rigorously in § 4. In §§ 5 and 6, practical possibilities of the method are discussed and are illustrated by some computer-simulated images. In some cases, the sign of the Burgers vector of the dislocation is shown to be found from the XTT images only.

## 2. The Green functions

Let a monochromatic X-ray bundle with the main wave vector $\mathbf{K}_0$ and infinitesimal lateral dimensions fall on a crystal surface. If the wave vector $\mathbf{K}_0$ satisfies the Bragg condition for the crystal net plane with reciprocal-

lattice vector **h**, the coherent superposition of the transmitted wave with wave vector close to $\mathbf{K}_0$ and the diffracted wave with wave vector close to $\mathbf{K}_h = \mathbf{K}_0 + \mathbf{h}$, will occur inside the crystal. Taking the directions $\mathbf{K}_0$ and $\mathbf{K}_h$ as the axes of the oblique-angled coordinate system $(s_0 O s_h)$, one can write the incident bundle in the form

$$\mathscr{E}_0^{(\mathrm{vac})}(s_0,s_h) = \delta(s_h - \xi_h)\exp(iK_0 s_0) \tag{2.1}$$

and the wave field $\mathscr{E}(s_0,s_h)$ inside the crystal is determined by

$$\mathscr{E}(s_0,s_h) = \mathfrak{S}_{00}(s_0,s_h,\xi_0,\xi_h)\exp(iK_0 s_0) + \mathfrak{S}_{h0}(s_0,s_h,\xi_0,\xi_h)\exp(iK_h s_h). \tag{2.2}$$

Here and below $(s_0,s_h)$ and $(\xi_0,\xi_h)$ denote the coordinates in the same single coordinate system used throughout this paper. Different symbols are used only to distinguish between the coordinates of the source location and of the observation point. For the standard diffraction geometry in (2.1) and (2.2), we use $(s_0,s_h)$ for the observation point and $(\xi_0,\xi_h)$ for the coordinates of the incident bundle on the entrance surface of the crystal and *vice versa* when considering the reciprocal diffraction geometry in § 4 (Fig. 1*a*,*b*). The amplitudes $\mathfrak{S}_{00}$ and $\mathfrak{S}_{h0}$ in (2.2) are the Green functions of the dynamical-diffraction problem by definition. Inside a crystal the wave field propagates between the directions of the transmitted and diffracted waves (the Borrmann fan) and, hence, the Green functions are equal to zero outside this region, *i.e.*

$$\mathfrak{S}_{00} = \mathfrak{S}_{h0} = 0, \quad \text{when } s_0 < \xi_0 \text{ or } s_h < \xi_h. \tag{2.3}$$

The representation (2.2) is analogous to the usual one of the diffraction theory in distorted crystals (Takagi, 1962, 1969) in the case of an incident wave of a particular kind (2.1). It is important that, owing to a small value of the crystal polarizability $\chi(\mathbf{r})$, the Green functions $\mathfrak{S}_{00}$ and $\mathfrak{S}_{h0}$ vary slowly at distances of the order of the X-ray wavelength. A characteristic alternation length of the Green functions with the depth inside a crystal is the extinction length

$$\Lambda = \frac{2\pi}{K_0}\left(\frac{\gamma_0\gamma_h}{\chi_h\chi_{-h}}\right)^{1/2} \simeq 10^5\,\lambda, \tag{2.4}$$

where $\chi_h$ is the Fourier component of $\chi(\mathbf{r})$, $\gamma_0$ and $\gamma_h$ are the cosines of the angles formed by the vectors $\mathbf{K}_0$ and $\mathbf{K}_h$ with the surface normal.

### 3. The diffracted intensity on XTT

In a general case, the incident X-ray wave has the form

$$\mathscr{E}_0^{(\mathrm{vac})}(s_0,s_h) = \mathscr{E}_0(s_h)\exp(iK_0 s_0). \tag{3.1}$$

Due to the linearity of dynamical diffraction equations, the wave-field amplitudes inside a crystal can be taken as the convolutions of the Green functions and the amplitude $\mathscr{E}_0(s_h)$ (the Huygens–Fresnel principle):

$$\mathscr{E}_0(s_0,s_h) = \oint \mathfrak{S}_{00}(s_0,s_h,\xi_0,\xi_h)\,\mathscr{E}_0(\xi_h)\,\mathrm{d}\xi_h; \tag{3.2}$$

$$\mathscr{E}_h(s_0,s_h) = \oint \mathfrak{S}_{h0}(s_0,s_h,\xi_0,\xi_h)\,\mathscr{E}_0(\xi_h)\,\mathrm{d}\xi_h;$$

with the integration going over the intersection line of the scattering plane with the entrance surface

$$\xi_0 = \xi_0(\xi_h) \tag{3.3}$$

and the diffracted intensity

$$I_h(s_0,s_h) = |\mathscr{E}_h(s_0,s_h)|^2 = \oint\oint \mathfrak{S}_{h0}[s_0,s_h,\xi_0(\xi_h),\xi_h] \times \mathfrak{S}^*_{h0}[s_0,s_h,\xi_0(\xi_h+s),\xi_h+s] \times \mathscr{E}_0(\xi_h)\,\mathscr{E}_0^*(\xi_h+s)\,\mathrm{d}\xi_h\,\mathrm{d}s. \tag{3.4}$$

Here and below the variable $s$ is the difference between two $\xi_h$ coordinates corresponding to two points on the entrance surface.

Now we will consider the characteristic features of XTT. In the XTT method, a homogeneous illumination of the crystal surface is achieved by scanning the crystal with a photographic plate across the primary beam (Lang, 1959). Because of this, the intensity (3.4) should be averaged with the observation time or, equivalently, with the positions of the X-ray point source. As a result, the product $\mathscr{E}_0(\xi_h)\mathscr{E}_0^*(\xi_h+s)$ should be substituted by its average value

$$\langle \mathscr{E}_0(\xi_h)\,\mathscr{E}_0^*(\xi_h+s)\rangle = I_0(\xi_h+s/2)\,\Gamma(s), \tag{3.5}$$

where $I_0(\xi_h)$ is the intensity distribution of the incident bundle, $\Gamma(s)$ is an autocorrelation function. The formula (3.5) holds for the stationary illumination condition and is valid when the intensity $I_0$ varies slowly with the correlation length $s_{\mathrm{cor}}$ of the incident bundle.

The intensity $I_h$ should also be averaged with the wavelength of the radiation used. The latter is usually the characteristic X-ray line of spectral width $\Delta\lambda/\lambda \simeq 10^{-3}$–$10^{-4}$, so that the dependence of the Green functions on the wavelength can be neglected if the crystal thickness $T$ is sufficiently small:

$$T \ll \Lambda\Big/\left(\frac{\Delta\Lambda}{\Lambda}\right) = \Lambda\Big/\left(\frac{\Delta\lambda}{\lambda}\right) \simeq (10^3\text{–}10^4)\,\Lambda. \tag{3.6}$$

[An inverse proportionality between the extinction length $\Lambda$ and $\lambda$ is taken into account in (3.6); see, for example, Pinsker, 1974.] In practice, (3.6) is always fulfilled.

Thus, only the autocorrelation function $\Gamma(s)$ should be averaged with the wavelength, which leads to some decrease of the correlation length.

From (3.5), the diffracted intensity takes the form

$$I_h(s_0,s_h) = \oint \mathrm{d}\xi_h\, I_{h0}[s_0,s_h,\xi_0(\xi_h),\xi_h]\, I_0(\xi_h), \qquad (3.7)$$

where $I_{h0}$ is the correlative Green function

$$I_{h0}[s_0,s_h,\xi_0(\xi_h),\xi_h] = \oint \mathfrak{S}^*_{h0}[s_0, s_h, \xi_0(\xi_h + s/2), \xi_h + s/2] \times \mathfrak{S}_{h0}[s_0,s_h, \xi_0(\xi_h - s/2),\xi_h - s/2]\, \Gamma(s)\, \mathrm{d}s. \qquad (3.8)$$

As an example, let us consider the case when the plane crystal is illuminated with an incoherent superposition of the plane waves with wave vectors in the range of lengths $(K_0 - \Delta K/2,\ K_0 + \Delta K/2)$ and with angular spread $\Delta\theta$. Let $\varphi$ be the angle between the wave vector and the normal to the surface. Then, for a single plane-wave component, one has

$$\mathscr{E}_0(\xi_h)\, \mathscr{E}^*_0(\xi_h + s) = \exp[(K \sin\varphi - K_0 \sin\varphi_0) \times s \sin 2\theta_B/\gamma_0].$$

In order to obtain the expression for $\Gamma(s)$ in an explicit form, one has to average the expression above with respect to $K$ and $\varphi$. Assuming $\Delta\theta \ll 1$, $\Delta K/K \ll 1$ and putting $\theta = \varphi - \varphi_0$, $k = K - K_0$, one finds immediately that the correlation function is given by

$$\Gamma(s) = \frac{1}{\Delta\theta}\int_{-\Delta\theta/2}^{\Delta\theta/2} \mathrm{d}\theta \exp(iK_0 \sin 2\theta_B\, s\theta) \times \frac{1}{\Delta K}\int_{-\Delta K/2}^{\Delta K/2} \mathrm{d}k \exp(ik \sin 2\theta_B\, s \tan\varphi_0)$$
$$= 2\frac{\sin(K_0 \sin 2\theta_B\, s\Delta\theta/2)}{K_0 \sin 2\theta_B\, s\Delta\theta} \times 2\frac{\sin(\Delta K \sin 2\theta_B\, s \tan\varphi_0/2)}{\Delta K \sin 2\theta_B\, s \tan\varphi_0} \qquad (3.9)$$

and has the form of the product of two factors, the first one depending only on the angular width of the incident bundle and the second one on the spectral width. With increase in $\Delta\theta$ or $\Delta K$, the correlation function tends to a $\delta$ function neglecting a normalization factor. Usually, in the XTT experiment $\Delta\theta \simeq 10^{-3}$–$10^{-4}$, $\Delta K/K_0 \simeq 10^{-3}$, $\lambda \simeq 10^{-10}$ m, and for both factors the correlation length is of the order of $10^{-6}$ m. In practice, the smaller of the two correlation lengths should be utilized to characterize the coherent properties of the bundle. Often, it is more convenient to deal with the correlation length $X_{\mathrm{cor}}$ along the entrance surface. The relation between $X_{\mathrm{cor}}$ and $s_{\mathrm{cor}}$ is evident:

$$X_{\mathrm{cor}} = s_{\mathrm{cor}} \sin 2\theta_B/\gamma_0. \qquad (3.10)$$

Any incident bundle can, in principle, be expanded in plane waves so that the above estimates are of general importance.

## 4. The reciprocity theorem

In light optics, the reciprocity theorem declares the following: a point source of unit strength located at a point $\mathbf{r}_1$ causes such an amplitude of the electromagnetic field at a point $\mathbf{r}_2$ as would be created at $\mathbf{r}_1$ by the same source located at $\mathbf{r}_2$ (Laue, 1935, 1960). A specific application of this statement in X-ray diffraction physics is that a wave field consists of separate components propagating in different directions and the amplitudes of these separate components must be known.

Kato (1968) pointed out that when the source and the observation points are sufficiently far from a crystal, the transmitted and diffracted waves are separate in space so that the reciprocity theorem may be applied to the diffracted wave only. The mutual permutation of the source and the observation points corresponds to the transition from standard to reciprocal diffraction geometry (Fig. 1). Considering the image on XTT as formed by scanning of a crystal with respect to an incident spherical wave of infinitesimal radius, Kato obtained from the reciprocity theorem that the intensity at a point $\mathbf{r}_p$ on XTT is equal to the integrated intensity of XST taken in the reciprocal geometry with a point source placed at $\mathbf{r}_p$.

The case of the spherical wave with an infinitesimal radius corresponds to a zero correlation length of the incident bundle. However, the more general case of partially coherent incident radiation is quite realistic. The consideration below enables one to estimate the accuracy of Kato's (1968) spherical-wave theory and to propose a more general approach. We shall prove the reciprocity theorem in the form of the relation between the Green functions for the standard and reciprocal diffraction geometries.

In order to derive this, let us introduce the Green functions $\mathfrak{S}_{00}$ and $\mathfrak{S}_{h0}$ as the solutions of the inhomogeneous Takagi equations with an X-ray point source:

$$i\frac{\partial}{\partial s_0}\mathfrak{S}_{00} + \eta_0\, \mathfrak{S}_{00} + \sigma_{-h} \exp(i\mathbf{hu})\, \mathfrak{S}_{h0} = i\,\delta(s_0 - \xi_0)\,\delta(s_h - \xi_h),$$
$$i\frac{\partial}{\partial s_h}\mathfrak{S}_{h0} + \eta_h\, \mathfrak{S}_{h0} + \sigma_h \exp(-i\mathbf{hu})\, \mathfrak{S}_{00} = 0, \qquad (4.1)$$

provided that they satisfy conditions (2.3).

In (4.1), $\mathbf{u}(\mathbf{r})$ is the displacement vector of the elastic field, $\sigma_{\pm h}$ are the normalized dynamical coefficients, $\eta_{0,h}$ are the geometrical factors (for notation see Chukhovskii & Petrashen', 1977). It is easily seen that the solutions of (4.1) and (2.3) satisfy the continuity conditions at the entrance surface $S_{\mathrm{ent}}$. Indeed, $S_{\mathrm{ent}}$ lies in the regions either $s_0 < \xi_0$ or $s_h < \xi_h$ and, owing to (2.3),

$$\mathfrak{S}_{h0}|_{S_{\mathrm{ent}}} = 0. \qquad (4.2)$$

Then, integrating the first equation (4.1) from $\xi_0 - \varepsilon$ to $\xi_0 + \varepsilon$ and allowing $\varepsilon$ to tend to zero, one finds that just under the entrance surface

$$\mathfrak{S}_{00}|_{S_{ent}} = \delta(s_h - \xi_h), \tag{4.3}$$

which, with (2.2), is in accordance with the incident bundle (2.1).

In the reciprocal geometry, the incident beam propagates along the axis $Os_h$ in a backward direction as does the diffracted beam along the axis $Os_0$, whereas the diffraction vector **h** remains the same. Thus, the Green functions $\tilde{\mathfrak{S}}_{00}$ and $\tilde{\mathfrak{S}}_{h0}$ for the reciprocal geometry satisfy the equations

$$\begin{aligned} &-i\frac{\partial}{\partial \xi_h}\tilde{\mathfrak{S}}_{00} + \eta_h \tilde{\mathfrak{S}}_{00} + \sigma_{-h}\exp(i\mathbf{hu})\,\tilde{\mathfrak{S}}_{h0} \\ &\quad = i\,\delta(\xi_h - s_h)\,\delta(\xi_0 - s_0), \qquad (4.4) \\ &-i\frac{\partial}{\partial \xi_0}\tilde{\mathfrak{S}}_{h0} + \eta_0 \tilde{\mathfrak{S}}_{h0} + \sigma_h \exp(-i\mathbf{hu})\,\tilde{\mathfrak{S}}_{00} = 0. \end{aligned}$$

Here, the entrance point is denoted as $(s_0, s_h)$ and the coordinates of an observation point as $(\xi_0, \xi_h)$. As a consequence, the Green functions $\tilde{\mathfrak{S}}_{00}$ and $\tilde{\mathfrak{S}}_{h0}$ are defined within the same region (2.3) as the Green functions $\mathfrak{S}_{00}$ and $\mathfrak{S}_{h0}$.

By means of the substitutions

$$\mathfrak{S}_{ij} = \exp[i\eta_0(s_0 - \xi_0) + i\eta_h(s_h - \xi_h)]\,G_{ij}, \tag{4.5}$$

the hyperbolic equations for the functions $G_{h0}$ and $\tilde{G}_{h0}$ are readily obtained:

$$\begin{aligned} &\frac{\partial}{\partial s_0}\left(e^{i\mathbf{hu}}\frac{\partial}{\partial s_h}G_{h0}\right) + \sigma^2 e^{i\mathbf{hu}} G_{h0} \\ &\quad = i\sigma_h\,\delta(s_0 - \xi_0)\,\delta(s_h - \xi_h), \qquad (4.6) \\ &\frac{\partial}{\partial \xi_h}\left(e^{i\mathbf{hu}}\frac{\partial}{\partial \xi_0}\tilde{G}_{h0}\right) + \sigma^2 e^{i\mathbf{hu}}\tilde{G}_{h0} \\ &\quad = i\sigma_h\,\delta(s_0 - \xi_0)\,\delta(s_h - \xi_h), \qquad (4.7) \end{aligned}$$

where $\sigma^2 = \sigma_h \sigma_{-h}$.

The integration of (4.6) from $\xi_0 - \varepsilon$ to $s_0$ and further from $\xi_h - \varepsilon$ to $s_h$ taking (2.3) into account turns (4.6) into the corresponding Volterra's integral equation of the second kind

$$\begin{aligned} &G_{h0} + \sigma^2 \int_{\xi_h - \varepsilon}^{s_h} e^{-i\mathbf{hu}} \int_{\xi_0 - \varepsilon}^{s_0} e^{i\mathbf{hu}} G_{h0}\,ds_0'\,ds_1' \\ &\quad = i\sigma_h\, e^{-i\mathbf{hu}}\,\theta(s_0 - \xi_0)\,\theta(s_h - \xi_h). \qquad (4.8) \end{aligned}$$

In order to derive an equation of the type (4.7), it is necessary to differentiate (4.8) with respect to $\xi_0$, $\xi_h$. Introducing the notation

$$F = \frac{\partial}{\partial \xi_h}\left\{\exp[i\mathbf{hu}(\xi_0, \xi_h)]\,\frac{\partial}{\partial \xi_0}G_{h0}\right\}, \tag{4.9}$$

and taking into account (2.3), one finds

$$\begin{aligned} &F + \sigma^2 \int_{\xi_h - \varepsilon}^{s_h} e^{-i\mathbf{hu}} \int_{\xi_0 - \varepsilon}^{s_0} e^{i\mathbf{hu}} F\,ds_0'\,ds_h' \\ &\quad = i\sigma_h\,\delta(s_0 - \xi_0)\,\delta(s_h - \xi_h). \qquad (4.10) \end{aligned}$$

From (4.10), it follows immediately that the combination

$$\sigma^{-2}\exp[-i\mathbf{hu}(\xi_0, \xi_h)]\,[i\sigma_h\,\delta(s_0 - \xi_0)\,\delta(s_h - \xi_h) - F]$$

satisfies the same equation (4.8) as for $G_{h0}$ so that these functions are equal to each other

$$\begin{aligned} &\sigma^{-2}\exp[-i\mathbf{hu}(\xi_0, \xi_h)]\left(i\sigma_h\,\delta(s_0 - \xi_0)\,\delta(s_h - \xi_h)\right. \\ &\left. - \frac{\partial}{\partial \xi_h}\left\{\exp[i\mathbf{hu}(\xi_0, \xi_h)]\,\frac{\partial}{\partial \xi_0}G_{h0}\right\}\right) = G_{h0}. \qquad (4.11) \end{aligned}$$

Equation (4.11) is equivalent to (4.7) for $\tilde{G}_{h0}$ and, keeping in mind (4.5), one has

$$\mathfrak{S}_{h0}(s_0, s_h, \xi_0, \xi_h) = \tilde{\mathfrak{S}}_{h0}(\xi_0, \xi_h, s_0, s_h). \tag{4.12}$$

The relation (4.12) represents the reciprocity theorem which we require to prove. Equation (4.12), however, enables us now to interpret the Green function $\mathfrak{S}_{h0}$ as a solution of the diffraction problem for reciprocal geometry. It is interesting that in the case of zero correlation lengths, $s_{cor} = 0$, the correlative Green function [see (3.8)] is given by

$$I_{h0} = |\tilde{\mathfrak{S}}_{h0}|^2 \tag{4.13}$$

and has the sense of the intensity distribution in XST, also in a reciprocal geometry. Assuming $I_0(\xi_h) =$ constant in (3.7), one obtains Kato's (1968) theorem for the intensity in XTT. In the general case of non-vanishing correlation length for the correlative Green function, one gets

$$\begin{aligned} I_{h0} = &\int_{-\infty}^{\infty} |\tilde{\mathfrak{S}}_{h0}[\xi_0(\xi_h + s/2), \xi_h + s/2, s_0, s_h]|^2\,\Gamma(s)\,ds \\ &- \tfrac{1}{2}\int_{-\infty}^{\infty} |\tilde{\mathfrak{S}}_{h0}[\xi_0(\xi_h + s/2), \xi_h + s/2, s_0, s_h] \\ &- \tilde{\mathfrak{S}}_{h0}[\xi_0(\xi_h - s/2), \xi_h - s/2, s_0, s_h]|^2\,\Gamma(s)\,ds, \end{aligned} \tag{4.14}$$

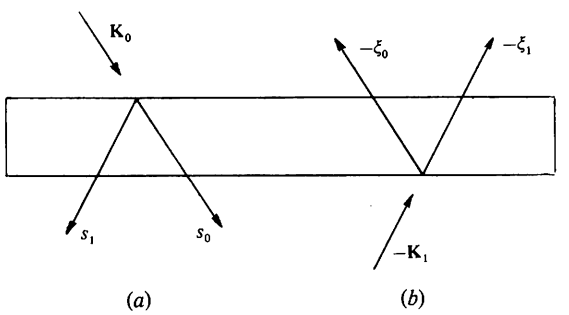


Fig. 1. Standard (*a*) and reciprocal (*b*) diffraction geometries.

taking into account the parity of the autocorrelation function $\Gamma(s)$.

Let $s_{cor}$ be small; then the integrated intensity can be written as

$$I_h(s_0,s_h) = s_{cor} \oint |\mathfrak{S}_{h0}|^2 \, d\xi_h - \tfrac{1}{2} \oint \oint |\mathfrak{S}_{h0}(\xi_h + s/2) - \mathfrak{S}_{h0}(\xi_h - s/2)|^2 \, \Gamma(s) \, ds \, d\xi_h$$
$$\simeq s_{cor}[\oint |\mathfrak{S}_{h0}|^2 \, d\xi_h - 0(\tfrac{1}{2} \oint |d\mathfrak{S}_{h0}/d\xi_h| \, d\xi_h) \, s_{cor}^2/24], \quad (4.15)$$

where the complete derivative $d\mathfrak{S}_{h0}/d\xi_h$ is taken along the entrance surface.

The second term on the right-hand side of (4.15) causes a decrease of the integrated intensity compared with Kato's result. The origin of this decrease becomes clear if one remembers that the non-zero correlation length is due to the finite angular spread of the incident beam, as was shown in § 3, whereas in Kato's theory this spread is infinite. The absolute value of the correction depends essentially on the rate of change of $\mathfrak{S}_{h0}$ on $S_{ent}$. For a perfect crystal of thickness $T$, the oscillation period of $\mathfrak{S}_{h0}$ decreases at the edges of the Borrmann fan down to a value of the order of $\Lambda^2/T$, so that a noticeable change of $I_h$ is possible when $s_{cor} \simeq 0{\cdot}1\Lambda$. Since for any distorted crystal the period of the *Pendellösung* fringes decreases (in comparison with a perfect crystal), the above correction of the integrated intensity increases. This effect leads to a reduction in the direct image contrast of a defect with increasing correlation length.

## 5. A comparative analysis of the XTT computer simulation

The formulae (3.7) and (3.8), the reciprocity theorem proven above and the numerical calculation of the Green function constitute the methodical basis of the problem.

Before going on to consider the XTT computer simulations of the dislocation image in detail, we shall discuss a different method not utilizing the reciprocity theorem, namely Cauchy's problem solution in the framework of the Takagi equations (Taupin, 1964; Authier, Malgrange & Tournarie, 1968) for incident plane waves and the subsequent averaging of the diffracted intensity by them (Epelboin, 1977).

It is shown below that the preference for one or other method depends on the relation between the correlation length and the necessary resolution on the simulated XTT.

The calculations based on the expansion of the incident bundle in a set of plane waves or a set of point sources may be considered as the particular cases of a more general method. In order to formulate it we shall assume that for numerical calculations a discrete network with triangular cells is used (Fig. 2, Takagi, 1962; Taupin, 1964). The size of the calculation step $\Delta_1$ depends mainly on the accuracy of the numerical method chosen. Let the lateral dimension of the illuminated area of a crystal be $(N-1)$ calculation steps. Then, the boundary conditions of the Cauchy problem are given at $N$ nodes of the net on the entrance surface. The size of the illuminated area is equal to $(N-1)\Delta_1 = A + Z$, where $A$ is the width of the simulated XTT and $Z$ is the crystal thickness (both quantities are measured along $Os_h$, as shown in Fig. 2).

Let the Cauchy problem be solved $M$ times for $M$ various distributions of the amplitudes and phases on the entrance surface. Any such distribution will be denoted by a vector $\mathbf{E}^{(m)} = \{E_n^{(m)}\}$ in the complex $N$-dimensional space. Every calculation gives an intensity distribution $I_n^{(m)}$ on the exit surface. From this, the average intensity distribution is given by

$$I_n = M^{-1} \sum_{m=1}^{M} I_n^{(m)}. \quad (5.1)$$

The only condition for the vectors $\mathbf{E}^{(m)}$ is that the autocorrelation function

$$\Gamma(i-j) = 2 \sum_{m=1}^{M} E_i^{(m)} E_j^{(m)*} / \sum_{m=1}^{M} (|E_i^{(m)}|^2 + |E_j^{(m)}|^2) \quad (5.2)$$

should correspond to the correlation length $s_{cor}$. In all other respects, values of $E_n^{(m)}$ are arbitrary. In such an approach, the correlation length $s_{cor}$ cannot be made smaller than $\Delta_1$. At the limit of $s_{cor} = \Delta_1$, all the correlators $\Gamma(i-j)$ with $i \neq j$ must be zero and, hence, the matrix $E_n^{(m)}$ must consist of columns orthogonal to each other, which is possible if $M \geq N$. In the simplest case of $M = N$, $E_n^{(m)} = \delta_{mn}$, which corresponds to a set of point sources.

In a more general case, when $s_{cor} \geq \Delta_1$, the minimum value of $M$ is defined as

$$M \gtrsim (\Delta_1/s_{cor}) N \simeq (A + Z)/s_{cor}. \quad (5.3)$$

This procedure may be improved by taking into account the fact that waves emitted from two points on the entrance surface at a distance greater than $Z$ from each other do not interfere so that the correlators $\Gamma(i-j)$ for $|i-j| > N_z = Z/\Delta_1$ have no influence on

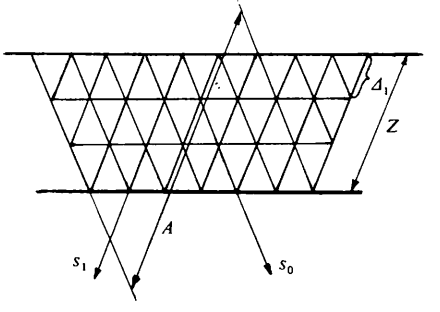


Fig. 2. A discrete network for the solution of the Cauchy problem.

the results and are non-essential being non-zero. Therefore, the minimum value of $M$ is

$$M \gtrsim (\Delta_1/s_{cor})\, N_z \simeq Z/s_{cor}. \tag{5.4}$$

In order to estimate the computer time needed, we shall assume that it is proportional to the number of net nodes multiplied by $M$;

$$L_1 = \frac{Z(A + Z/2)}{\Delta_1^2} M \simeq \frac{(A + Z/2)\, Z^2}{\Delta_1^2\, s_{cor}}. \tag{5.5}$$

In the method proposed on the basis of the reciprocity theorem, every one of the Green functions for the reciprocal geometry is calculated in a triangular area (the Borrmann fan) containing the net nodes

$$L_G = Z^2/2\Delta_2^2 \tag{5.6}$$

($\Delta_2$ is the calculation step size).

The time needed for averaging (3.8) with a finite correlation length $s_{cor}$ is proportional to $Zs_{cor}/\Delta_2^2$ and is much less than $L_G$. The total computing time is defined as

$$L_2 = AZ^2/2\Delta_2^2\alpha, \tag{5.7}$$

where $\alpha$ is an average distance between the computing points on XTT.

By use of (5.5), (5.7), the time ratio for the two methods involved is

$$\frac{L_1}{L_2} = \frac{2\alpha}{s_{cor}} \frac{(A + Z/2)}{A} \left(\frac{\Delta_2}{\Delta_1}\right)^2. \tag{5.8}$$

Taking as the typical simulation values $s_{cor} \simeq 10^{-6}$ m, $\alpha \simeq 10^{-5}$ m, $A \simeq Z$, one finds $L_1/L_2 \simeq 30(\Delta_2/\Delta_1)^2$. The ratio $\Delta_2/\Delta_1$ depends on several factors. The calculation of the Green functions can be carried out by means of a net with an alternating step size (Petrashen', 1976) and the comparable accuracy of a single integration is achieved when $\Delta_2$ is at least twice as large as $\Delta_1$. Furthermore, as a rule the correlation length $s_{cor}$ is smaller than the step size $\Delta_1$ chosen for the numerical solution of the Cauchy problem (Authier, Malgrange & Tournarie, 1968; Epelboin, 1974). As a consequence, good agreement with the XTT experiment is impossible without some additional reduction of $\Delta_1$ beyond the requirements of the accuracy of the integration procedure itself. Furthermore, in practice, the autocorrelation function $\Gamma(s)$ should be some smooth function provided that the correlation length is comparable with the minimum period of the *Pendellösung* fringes, otherwise the simulation results may be unstable with respect to the changes of $\Delta_1$ or $s_{cor}$, as was shown by Epelboin (1977). The stability condition may be satisfied only if $\Delta_1 \ll s_{cor}$.

Thus, the above treatment shows that for typical XTT experiment conditions, the numerical solution of the Cauchy problem requires a time a few hundred times greater than that needed in the case of the proposed method, based on the reciprocity theorem. This means several hundred hours on a middle-class computer, which is quite unrealistic. Nevertheless, the Cauchy method is so much the better when the correlation length is larger and is certainly the best one for double-crystal topography.

## 6. The applications of the theory

There are a few examples to provide illustrations of the theory applications (Petrashen' & Chukhovskii, 1978; Petrashen', Chukhovskii & Shulpina, 1978). We shall compare below the experimental and computed intensity profiles for dislocations parallel to the crystal surface. In Fig. 3(*a*), (*b*), two experimental XTT of a chosen area of a single crystal of Si are taken of the reflections $\bar{4}22$ and $42\bar{2}$ with Mo $K\alpha$ radiation. For dislocations parallel to the surface, changing the sign of the diffraction vector is equivalent to changing the sign of the Burgers vector **b** of the dislocation. So the pairs of XTT with opposite diffraction vectors **h**, $-$**h** are very convenient for investigating the dependence of the XTT images on the sign of a dislocation. Of the two dislocation images shown in Fig. 3(*a*), (*b*), one corre-

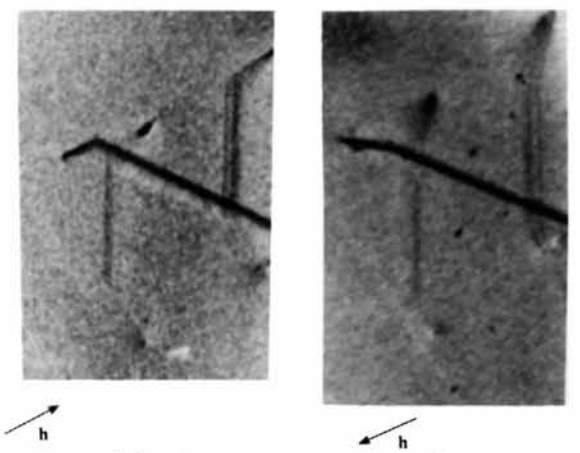


Fig. 3. XTT of dislocations in 900 μm thick Si crystal, taken for $\bar{4}22$(*a*) and $42\bar{2}$(*b*) reflections.

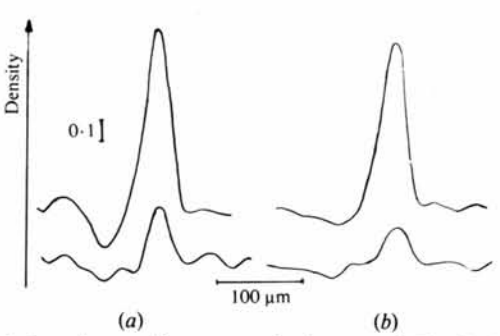


Fig. 4. Intensity profiles across the images of Fig. 3. (*a*) $\bar{4}22$ reflection. (*b*) $42\bar{2}$ reflection.

sponds to a screw dislocation with $|(\mathbf{h}.\mathbf{b})| = 3$ (stronger contrast) the other one (at 60° to the first) to a dislocation with $|(\mathbf{h}.\mathbf{b})| = 1$ (weaker contrast). The corresponding photometric profiles are shown in Fig. 4.

The calculations (Fig. 5) have been performed on a middle-class computer (M-4030, the computation speed is about $10^5$ op/s). The general principles of the numerical procedure have been given by Petrashen' (1976) and further details will be published elsewhere. To calculate the Green functions with the source at a point in the reciprocal geometry, the Borrmann fan is divided into integration cells forming a rhombic difference net (Fig. 6). In the middle of the net the step size is of the order of $0{\cdot}1A$, whereas towards the edges of the fan the step is reduced, which is very important for taking into account the rapid oscillations of the Green functions. At every step, the value of the Green function at the point $D$ of the subsequent integration cell is calculated by use of previously calculated values at the points $A$, $B$, $C$ (Fig. 6) in accordance with the difference formula

$$F_D - F_B = (F_C - F_A)\, e^{iw} - \frac{2\sigma^2 C^2 \Omega}{1 + \sigma^2 C^2 \Omega}\,(F_C\, e^{iw} + F_B),$$

where $\mathfrak{S}_{h0}$ and $F$ are related through the normal absorption factor

$$\mathfrak{S}_{h0} = F \exp(-\mu t/2 \cos\theta_B).$$

$C$ is the polarization factor, $4\Omega$ is the area of the integration cell, $\sigma^2 = 1 + 2i\kappa$, $\kappa$ is the normalized dynamical absorption coefficient, $w = \mathbf{h}(\mathbf{u}_{AC} - \mathbf{u}_{BD})$ is proportional to the local deviation from the Bragg condition within the cell $ABCD$. The boundary conditions require the function $F$ to be equal to 1 on the line $\xi_0 = s_0$ and $\exp\{-i\mathbf{h}[\mathbf{u}(\xi_0) - \mathbf{u}(s_0)]\}$ on the line $\xi_h = s_h$. Two Green's functions for two polarizations are calculated in parallel. The computation time for any of the profiles in Fig. 5 was about 1 h. This shows the big improvement in time with the new method proposed (*cf.* Epelboin, 1977).

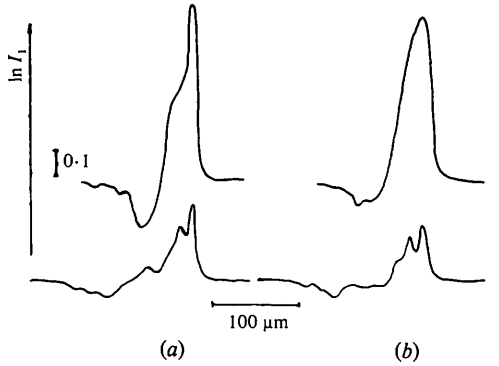


Fig. 5. Computed intensity profiles for the experimental conditions of the XTT of Fig. 3. (*a*) $\bar{4}22$ reflection. (*b*) $4\bar{2}\bar{2}$ reflection.

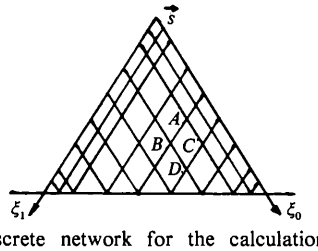


Fig. 6. A discrete network for the calculation of the Green functions.

In all the four cases considered, a good agreement between the theoretical and experimental profiles is seen for the relative peaks of the intensities and the depths of the dynamical shadows.

The fact of principal importance is that there is a very noticeable difference in the intensities of the direct images in the case of 60° dislocation with $(\mathbf{h}.\mathbf{b}) = \pm 1$. This enables one to determine the sign of the Burgers vector. For the screw dislocation with $|(\mathbf{h}.\mathbf{b})| = 3$, the peak intensity is weakly dependent on the sign of $(\mathbf{h}.\mathbf{b})$. The physical reason for the phenomenon is that the two different scattering processes are responsible for the formation of the direct images (Petrashen' & Chukhovskii, 1978): the kinematical scattering due to the strong distortions close to the dislocation line is independent of the sign of a deformation, while the dynamical scattering prevails in the weakly distorted regions and is sensitive to the sign of the strain gradient due to the anomalous absorption effect. With increase of $|(\mathbf{h}.\mathbf{b})|$, the diffracted intensity scattered kinematically increases rapidly and masks the sign-dependent dynamical contribution. The present experimental data confirm this statement.

From the comparison of Figs. 4 and 5 it is seen that the depth of the dynamical shadow of the dislocation profiles may also be sensitive to the sign of the Burgers vector. The physical interpretation of this result is much more complicated and may be the subject of a separate study.

The above considerations of the problem in question lead us to the conclusion that the computer simulation of XTT based on the theory proposed can be a powerful tool in current XTT experiments.

## References

AUTHIER, A. (1967). *Adv. X-ray Anal.* **10**, 9–31.

AUTHIER, A., MALGRANGE, C. & TOURNARIE, M. (1968). *Acta Cryst.* A**24**, 126–136.

BALIBAR, F. & AUTHIER, A. (1967). *Phys. Status Solidi*, **21**, 413–422.

CHUKHOVSKII, F. N. & PETRASHEN', P. V. (1977). *Acta Cryst.* A**33**, 311–319.

CHUKHOVSKII, F. N. & SHTOLBERG, A. A. (1970). *Phys. Status Solidi*, **41**, 815–825.

CHUKHOVSKII, F. N. & SHTOLBERG, A. A. (1973). *Phys. Status Solidi B*, **56**, K97–K99.

EPELBOIN, Y. (1974). *J. Appl. Cryst.* **7**, 372–377.
EPELBOIN, Y. (1977). *Acta Cryst.* A**33**, 758–767.
KATO, N. (1968). *Acta Cryst.* A**24**, 157–160.
KATO, N. & LANG, A. R. (1959). *Acta Cryst.* **12**, 787–794.
LANG, A. R. (1959). *Acta Cryst.* **12**, 249–250.
LAUE, M. VON (1935). *Ann. Phys. (Leipzig)*, **23**, 705.
LAUE, M. VON (1960). *Röntgenstrahlinterferenzen.* Frankfurt am Main: Akademische Verlagsges.
PETRASHEN', P. V. (1976). *Fiz. Tverd. Tela*, **18**, 3729–3731.
PETRASHEN', P. V. & CHUKHOVSKII, F. N. (1978). *Fiz. Tverd. Tela*, **20**, 1104–1108.
PETRASHEN', P. V., CHUKHOVSKII, F. N. & SHULPINA, I. L. (1978). *Dokl. Akad. Nauk SSSR*, **240**, 84–87.
PINSKER, Z. G. (1974). *The X-ray Dynamical Scattering by Perfect Crystals.* Moscow: Nauka. (In Russian.)
TAKAGI, S. (1962). *Acta Cryst.* **15**, 1311–1312.
TAKAGI, S. (1969). *J. Phys. Soc. Jpn*, **26**, 1239–1253.
TAUPIN, D. (1964). *Bull. Soc. Fr. Minéral. Cristallogr.* **87**, 469–511.
WONCIEWICZ, B. C. & PATEL, J. R. (1975). *J. Appl. Cryst.* **8**, 67–68.
WONCIEWICZ, B. C. & PATEL, J. R. (1976). *J. Appl. Phys.* **47**, 1837–1845.

*Acta Cryst.* (1980). A**36**, 295–298

# On the Fourier Refinement of Protein Structures

BY M. VIJAYAN

*Molecular Biophysics Unit,* Indian Institute of Science, Bangalore* 560 012, *India and Laboratory of Molecular Biophysics, South Parks Road, Oxford, England*

(*Received* 20 *April* 1979; *accepted* 12 *November* 1979)

## Abstract

The situation normally encountered in the high-resolution refinement of protein structures is one in which the inaccurate positions of $P$ out of a total of $N$ atoms are known whereas those of the remaining atoms are unknown. Fourier maps with coefficients $(F_N - F'_P) \times \exp(i\alpha'_P)$ and $(mF_N - nF'_P) \exp(i\alpha'_P)$, where $F_N$ is the observed structure factor and $F'_P$ and $\alpha'_P$ are the magnitude and the phase angle of the calculated structure factor corresponding to the inaccurate atomic positions, are often used to correct the positions of the $P$ atoms and to determine those of the $Q$ unknown atoms. A general theoretical approach is presented to elucidate the effect of errors in the positions of the known atoms on the corrected positions of the known atoms and the positions of the unknown atoms derived from such maps. The theory also leads to the optimal choice of parameters used in the different syntheses. When the errors in the positions of the input atoms are systematic, their effects are not taken care of automatically by the syntheses.

## Introduction

Fourier methods are extensively used at different stages of the high-resolution refinement of proteins to calculate the shifts in structural parameters as well as to check the results obtained during the course of the refinement (Freer, Alden, Carter & Kraut, 1975; Watenpaugh, Sieker, Herriot & Jensen, 1973; Bode & Schwager, 1975; Dodson, Dodson, Hodgkin, Isaacs & Vijayan, 1978). The problems associated with these methods become more pronounced when they are applied to protein crystallography for several reasons. They often give rise to phenomena which cannot be anticipated or easily defined, and one can arrive at a crystallographically acceptable, but erroneous, refined structure (Dodson *et al.*, 1978). Hence the need for a fresh theoretical look at Fourier methods.

## Modulus synthesis, phase synthesis and their convolution

Fourier methods have been analysed by many workers (*e.g.* Luzzati, 1953; Ramachandran & Srinivasan, 1970; Dodson & Vijayan, 1971). The formulation of Ramachandran & Srinivasan is used in the present analysis and the relevant results from their work are outlined in this section.

If the structure consists of $N$ atoms with positions $\mathbf{r}_j$ and form factors $f_j$ ($j = 1, \ldots, N$), a Fourier synthesis with the structure factors $F \exp(i\alpha)$ as coefficients obviously has peaks at $\mathbf{r}_j$ with strengths proportional to $f_j$. If the moduli of the structure factors are used as Fourier coefficients, Ramachandran & Srinivasan have shown, to a first approximation, that the resulting

* Contribution No. 144.

0567-7394/80/020295-04$01.00 